Article

Cell Host & Microbe

The Marburgvirus-Neutralizing Human Monoclonal Antibody MR191 Targets a Conserved Site to Block Virus Receptor Binding

Graphical Abstract

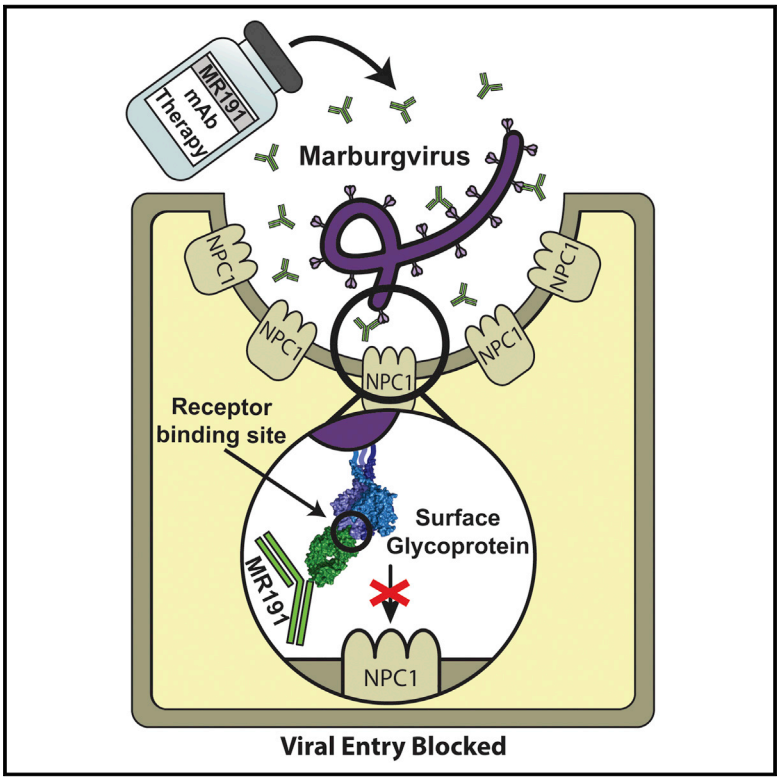

Authors

Liam B. King, Marnie L. Fusco, Andrew I. Flyak, ..., Alexander Bukreyev, James E. Crowe, Jr., Erica Ollmann Saphire

Correspondence

erica@scripps.edu

In Brief

Using structural analysis, King et al. demonstrate how the protective, potentially therapeutic, monoclonal antibody MR191 engages the marburgvirus glycoprotein receptor-binding site. The resulting complex is able to outcompete the host entry receptor NPC1 for viral neutralization. In addition, the structure illuminates previously disordered, functionally critical regions of the marburgvirus glycoprotein.

Highlights

- 3.2 Å structure of mAb MR191 complexed with trimeric marburgvirus surface glycoprotein
- MR191 neutralizes by occupying the conserved receptor-binding site
- MR191 competes with the host receptor Niemann-Pick C1
- Escape mutants map outside the MR191 footprint, suggesting effect on quaternary structure

King et al., 2018, Cell Host & Microbe *23*, 101–109
January 10, 2018 © 2017 Elsevier Inc.
https://doi.org/10.1016/j.chom.2017.12.003

Cell Host & Microbe
Article

The Marburgvirus-Neutralizing Human Monoclonal Antibody MR191 Targets a Conserved Site to Block Virus Receptor Binding

Liam B. King,[1] Marnie L. Fusco,[1] Andrew I. Flyak,[2,9] Philipp A. Ilinykh,[3,7] Kai Huang,[3,7] Bronwyn Gunn,[4] Robert N. Kirchdoerfer,[1] Kathryn M. Hastie,[1] Amandeep K. Sangha,[5] Jens Meiler,[5] Galit Alter,[4] Alexander Bukreyev,[3,6,7] James E. Crowe, Jr.,[2] and Erica Ollmann Saphire[1,8,10,*]
[1]Department of Immunology and Microbiology, The Scripps Research Institute, La Jolla, CA 92037, USA
[2]Departments of Pediatrics, Pathology, Microbiology, and Immunology, and the Vanderbilt Vaccine Center, Vanderbilt University Medical Center, Nashville, TN 37232, USA
[3]Department of Pathology, University of Texas Medical Branch, Galveston, TX 77555, USA
[4]Ragon Institute of Massachusetts General Hospital, Massachusetts Institute of Technology and Harvard University, Cambridge, MA 02139, USA
[5]Department of Chemistry and Center for Structural Biology, Vanderbilt University, Nashville, TN 37232, USA
[6]Department of Microbiology & Immunology, University of Texas Medical Branch, Galveston, TX 77555, USA
[7]Galveston National Laboratory, Galveston, TX 77550, USA
[8]Skaggs Institute for Chemical Biology, The Scripps Research Institute, La Jolla, CA 92037, USA
[9]Present address: Division of Biology and Biological Engineering, California Institute of Technology, Pasadena, CA 91106, USA
[10]Lead Contact
*Correspondence: erica@scripps.edu
https://doi.org/10.1016/j.chom.2017.12.003

SUMMARY

Since their first identification 50 years ago, marburgviruses have emerged several times, with 83%–90% lethality in the largest outbreaks. Although no vaccines or therapeutics are available for human use, the human antibody MR191 provides complete protection in non-human primates when delivered several days after inoculation of a lethal marburgvirus dose. The detailed neutralization mechanism of MR191 remains outstanding. Here we present a 3.2 Å crystal structure of MR191 complexed with a trimeric marburgvirus surface glycoprotein (GP). MR191 neutralizes by occupying the conserved receptor-binding site and competing with the host receptor Niemann-Pick C1. The structure illuminates previously disordered regions of GP including the stalk, fusion loop, CX_6CC switch, and an N-terminal region of GP2 that wraps about the outside of GP1 to anchor a marburgvirus-specific "wing" antibody epitope. Virus escape mutations mapped far outside the MR191 receptor-binding site footprint suggest a role for these other regions in the GP quaternary structure.

INTRODUCTION

Filoviruses cause severe disease and have been responsible for multiple outbreaks among both humans and non-human primates. Within the filovirus family are three genera: *Ebolavirus* (which includes Ebola virus [EBOV], Sudan virus [SUDV], Bundibugyo virus, Taï Forest virus, and Reston virus), *Marburgvirus* (which includes Marburg virus [MARV] and Ravn virus [RAVV]), and *Cuevavirus*. Ebola virus disease (EVD) and Marburg virus disease (MVD) are clinically similar. MARV was the first filovirus identified, and has re-emerged multiple times since its 1967 discovery. The largest outbreak was nearly 90% lethal (CDC, 2005).

Antibody therapies are a promising avenue for prophylaxis, post-exposure prophylaxis, and therapeutic treatment of emerging viral diseases (Chanock et al., 1993; Zeitlin et al., 1999; Lachmann, 2012; Burton and Saphire, 2015). One antibody-based therapy, ZMapp (Qiu et al., 2014), appeared to be beneficial during the 2013–2016 EVD outbreak, although the results did not reach the threshold of statistical significance (PREVAIL II Writing Group et al., 2016). None of the antibodies in ZMapp reacts with marburgviruses, and at this time there are no approved treatments available for MVD.

Filoviruses produce enveloped virions that express a single glycoprotein (GP) on the surface. GP is responsible for attachment to and entry of target cells, and is the primary target for antibodies and vaccines (Dye et al., 2012). Filovirus GPs share a common core fold and trimeric organization, but are antigenically distinct. Marburgvirus GPs are only 30% identical to EBOV GP in primary amino acid sequence. The two marburgvirus GPs, however, MARV and RAVV GP, are quite similar to each other in sequence, and likely structure, with 78% amino acid identity overall and 90% identity outside the mucin-like domain.

Filovirus GPs are 676–681 amino acids in length and are cleaved in the producer cell to yield two subunits, GP1 and GP2, which remain anchored by a single disulfide bond (Volchkov et al., 1998, 2000). The larger GP1 subunit harbors a receptor-binding core, a "glycan cap" subdomain, and a C-terminal, heavily glycosylated mucin-like domain. GP2 contains the membrane fusion machinery, including the internal

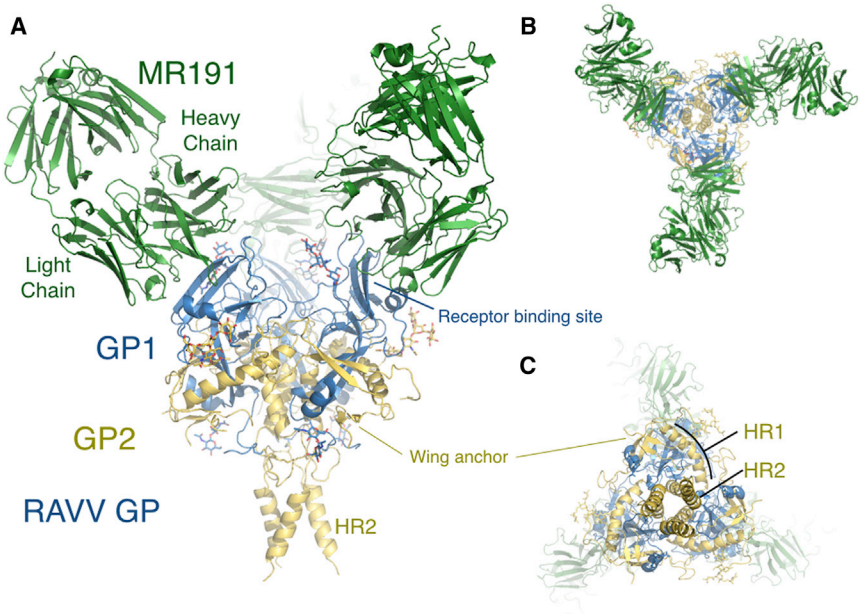

Figure 1. Structure of RAVV GP-MR191 Complex

Complete RAVV trimeric GP is illustrated in complex with three MR191 Fab fragments.

(A) The heavy chain of each Fab (green) binds into the hydrophobic receptor-binding pocket of GP1 (blue). GP2 is colored gold. Visible glycans are colored with carbon atoms blue for those attached to GP1 and gold for those attached to GP2. Oxygen atoms are red.

(B) Top view, from antibody perspective looking onto viral surface.

(C) Bottom view, viewing from the viral membrane outwards. The trimeric bundle of HR2 helices is visible at center with HR1 to the outside.

fusion loop (IFL), two heptad repeat regions (HR1 and HR2), and a transmembrane domain to anchor the protein in the viral membrane (Bukreyev et al., 1993; Feldmann et al., 1993; Lee et al., 2008). After attachment, filoviruses enter cells via macropinocytosis (Nanbo et al., 2010; Saeed et al., 2010; Aleksandrowicz et al., 2011; Mulherkar et al., 2011). Once in the endosome, ebolavirus GPs are cleaved by cathepsins B and/or L (Chandran et al., 2005). Cleavage removes the heavily glycosylated glycan cap and mucin-like domains from ebolavirus GP1, and is required to expose the binding site for the entry receptor, Niemann-Pick C1 (NPC1) (Chandran et al., 2005; Schornberg et al., 2006; Hood et al., 2010; Brecher et al., 2012; Marzi et al., 2012). Interestingly, marburgviruses use the same NPC1 receptor but do not share the dependence on cathepsins B and L of ebolaviruses (Gnirss et al., 2012).

The shared NPC1 receptor is an endosomal/lysosomal 13-pass transmembrane protein with three large luminal domains, A, C, and I, of which domain C (NPC1-C) is necessary and sufficient for filovirus binding (Carette et al., 2011; Miller et al., 2012; Gong et al., 2016). Recent work has shown that the interaction between EBOV GP and NPC1-C is mediated by two protruding loops of NPC1-C, which engage a hydrophobic pocket on the surface of cleaved GP (GPcl) (Wang et al., 2016). Prior to cleavage, an 86 amino acid "glycan cap" occupies the NPC1-binding site on EBOV GP (Lee et al., 2008). Hence, uncleaved ebolavirus GPs do not bind to NPC1-C (Miller et al., 2012).

Potent antibodies against marburgvirus recently were isolated from circulating B cells in the blood of a human survivor of natural MVD (Flyak et al., 2015). Among these, antibody MR191 was shown to protect non-human primates against a lethal marburgvirus challenge when treatment was initiated as late as 5 days post-exposure (Mire et al., 2017). In that study, MR191 provided protection superior to that of two other antibodies in the same competition group, MR78 and MR82 (Mire et al., 2017). Here, we present the crystal structure at 3.2 Å resolution, of trimeric, uncleaved, pre-fusion RAVV GP in complex with antibody MR191 (PDB: 6BP2). This structure is higher in resolution than the marburgvirus GP structure previously available. The higher-resolution map reveals that the N-terminal region of marburgvirus GP2 wraps around the outside of the GP core, to occupy a position that, in ebolaviruses, is instead held by GP1. This newly visualized subdomain of GP2 anchors a marburgvirus-specific "wing" epitope: the only other epitope that has been yet shown to elicit protective antibodies against MVD (Fusco et al., 2015). This structure also now illustrates the complete IFL, GP1-GP2 disulfide anchor, CX_6CC switch region, and HR2 stalk of RAVV GP, all of which were disordered in structures obtained previously. Fundamental differences between marburgviruses and ebolaviruses in the organization of the GP2 wing and the glycosylated regions in GP1 help explain why marburgvirus entry is cathepsins B- and L-independent, and why it elicits a different pattern of antibody reactivity than ebolaviruses.

Further, the crystal structure illustrates that the potent therapeutic antibody MR191 binds into the receptor-binding site near the apex of GP1. In ebolaviruses, this site is inaccessible due to the position of the glycan cap in the absence of cathepsin cleavage. However, in the marburgvirus GP, the polypeptide region equivalent to the ebolavirus glycan cap appears to be flexible and does not as effectively block antibody access to the receptor-binding site. MR191 competes with NPC1-C for binding of GP and appears to mimic NPC1-C (Wang et al., 2016) in its attachment. Contact residues for MR191 are also essential for receptor binding and are highly conserved among related filoviruses. The conservation and importance of the MR191 binding site suggests that the footprint of MR191 may be somewhat more resistant to mutagenic escape than other, less-conserved antibody epitopes. Interestingly, the escape mutations that arose during cell culture passage occurred in distant sites, suggesting an allosteric communication or an as-yet unknown role of these regions in maintenance of GP quaternary structure.

RESULTS

3.2 Å Structure of RAVV GP

Recombinant RAVV GP ectodomain (residues 1–636, with 257–425 deleted to remove the mucin-like domain) was

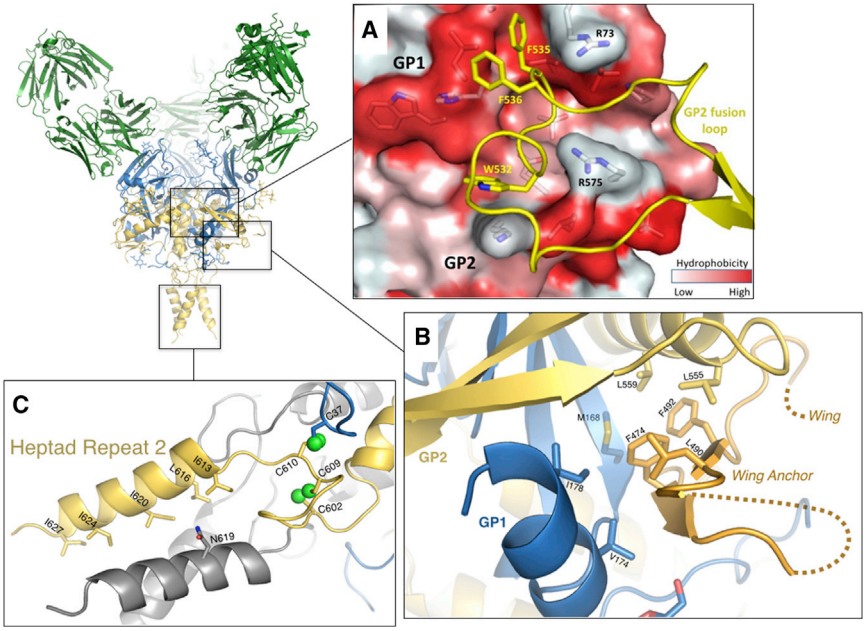

Figure 2. New Features of a Marburgvirus GP

New elements revealed in RAVV GP.

(A) The internal fusion loop (yellow) is shown coordinating with GP1 of the neighboring monomer within the trimer. The adjacent GP is shown in surface representation and is colored by hydrophobicity. Residues W532, F535, and F536 of the fusion peptide bind into hydrophobic pockets (red).

(B) The GP2 wing anchor (orange) fits between GP1 (blue) and GP2 (gold). L490, F474, and F492 form hydrophobic contacts to secure the wing against the GP1-GP2 core.

(C) The C-terminal heptad repeat 2 (HR2) of GP2 is resolved to residue 629, and illustrates hydrophobic packing among central residues I613, L616, I620, I624, and I627. The GP1-GP2 disulfide bond (residue C37-C610) and the GP2-GP2 disulfide bond (C602-C609) are visible in this higher-resolution structure, indicated with green spheres as sulfur atoms.

expressed in *Drosophila* S2 cells, purified, and complexed with Fab fragments of the human MR191 antibody for crystallization. Data to 3.2 Å were collected from cryo-protected crystals at beamline 23-ID-D of the Advanced Photon Source. Residues 33–180 of GP1, 469–629 of GP2, and glycans attached to N94, N171, and N564 were visible. Residues 2–216 of the light chain and 2–227 of the heavy chain of MR191 also were visible. One GP protomer-Fab complex is contained in the asymmetric unit of the P321 crystals, with the biologically relevant trimer formed about a crystallographic 3-fold axis (Figure 1 and Table S1).

The structure illuminates functionally critical regions of marburgvirus GP (Figure 2) that were disordered in the previous marburgvirus GP structure. First, the IFL of GP2 (residues 514–551) can now be traced in its entirety (Figure 2A). The IFL is anchored to the protein core via an anti-parallel β strand scaffold, with a 20-residue loop containing the hydrophobic fusion peptide. The IFL rests in the GP1/GP2 interface of the adjacent protomer in the GP trimer, and is secured by several hydrophobic interactions and hydrogen bonds.

Second, we can now visualize an N-terminal region of GP2, beginning 34 residues downstream of the furin cleavage site and including residues 469–478 and 487–498. These residues anchor the marburgvirus-specific "wing" domain, residues 436–501. This site is targeted by marburgvirus-specific protective antibodies (Fusco et al., 2015), and is the only major recognition site of antibodies against marburgviruses yet described, beyond the receptor-binding site. We were able to place the GP2 wing anchor at the base of GP unambiguously, packing against the GP1 core directly beneath the C terminus of the fusion loop and the start of heptad repeat 1 (HR1) (Figure 2B). This observation was unexpected, since this same site on the GP1 core of EBOV or SUDV is not bound by any part of GP2, but instead by residues 32–45 at the N terminus of GP1 (Figure S5). The wing domain is unique to marburgviruses and results from a 66-residue N-terminal shift in the position of the furin cleavage event (R501 in EBOV, but R435 in MARV), which separates the GP1 and GP2 segments. Therefore, residues at the equivalent sequence region are included in the ebolavirus mucin-like domain and attach to the top of GP1 in ebolaviruses, not to GP2 as in marburgviruses.

The crystal structure also revealed the structure of the heptad repeat 2 (HR2) region, which forms the "stalk" between the GP core and the viral membrane (Figure 2C). Here, HR2 forms a three-helix bundle with five hydrophobic residues from each helix facing inward to form a hydrophobic core, likely stabilizing the trimer. Although these residues differ in sequence from those of ebolaviruses, the hydrophobic packing is conserved (Zhao et al., 2016). Further, an N-linked glycosylation sequon is present in the HR2 of all known filoviruses. This glycan has been visualized for EBOV (Zhao et al., 2016), and likely shields a portion of this conserved site from antibody recognition. Although an NXS glycosylation sequon is present in the sequence of all marburgvirus isolates, a glycan is not visible in this structure, and there does not appear to be enough space for a glycan attached at this site to fit within in the crystal packing. It is unknown if this site is glycosylated on authentic marburgvirus particles. Immediately prior to HR2, the CX_6CC disulfide-bearing switch region also can be seen in its entirety. The first and second cysteines in this motif (Cys-602 and Cys-609) form an intra-GP2 disulfide bond that anchors the switch region in a 360° turn as it descends downward to the membrane. The third cysteine in this motif (Cys-610) forms the disulfide anchor to GP1 (Cys-37).

Absence of an Ordered Glycan Cap

In all structures of uncleaved, mucin-deleted EBOV or SUDV GP, a glycan cap subdomain of GP1 occupies the hydrophobic NPC1-C binding pocket (Lee et al., 2008; Dias et al., 2011; Bale et al., 2012; Misasi et al., 2016; Pallesen et al., 2016; Zhao et al., 2016). The equivalent residues for marburgviruses (174–256) are included in proteins used for crystallization in

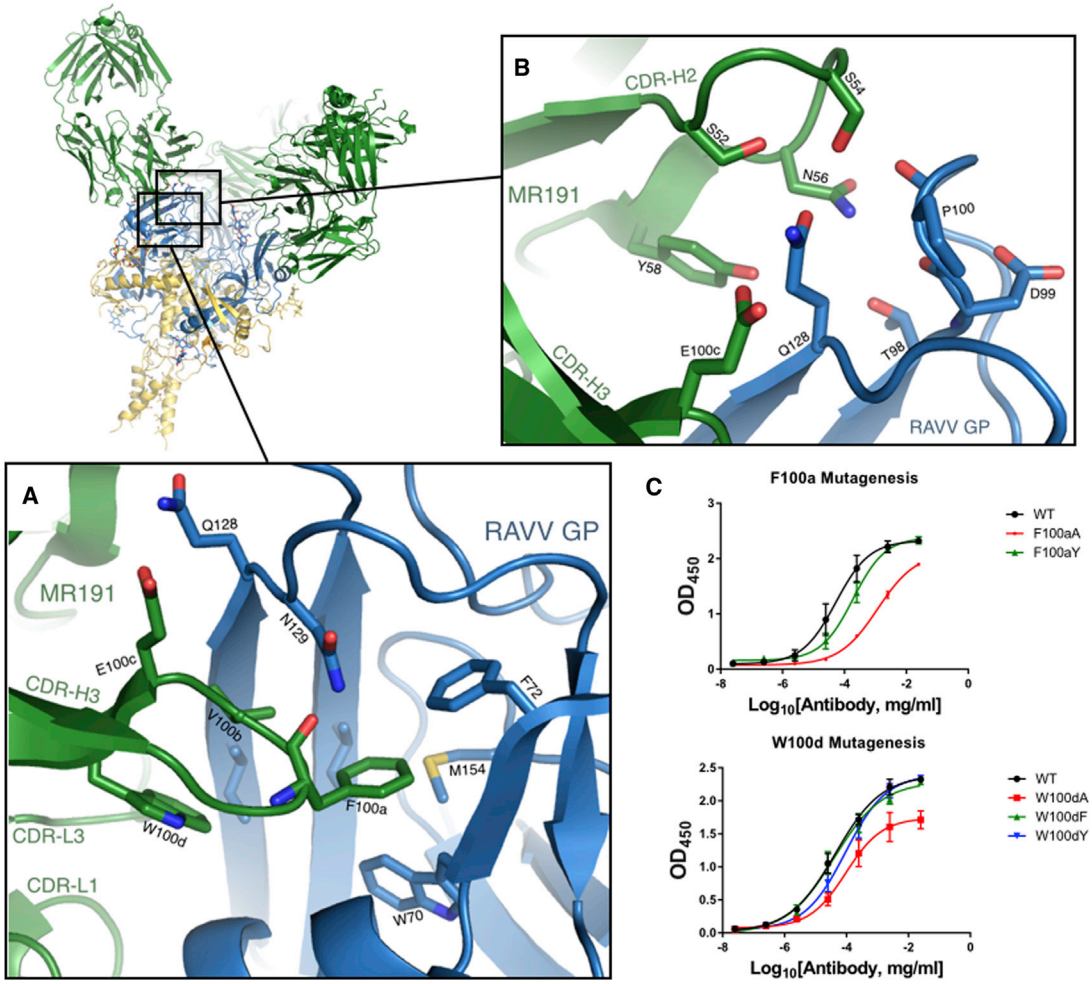

Figure 3. Receptor-Binding Site and Crest Interactions

MR191 binds into the receptor-binding site of RAVV GP.

(A) CDR H3 of MR191 (green) engages the hydrophobic trough with F100a binding deepest within the pocket.

(B) CDR-H2 of MR191 engages the crest of GP. Residues S52, S54, N56, and Y58 form hydrogen bonds with both the main chain of RAVV GP and side chains of Q128 and T98.

(C) Mutagenesis of key hydrophobic residues of CDR-H3. Top, MR191 bearing mutations to residue F100a, and bottom, MR191 bearing mutations to W100d evaluated for binding to RAVV GP. A hydrophobic-aromatic residue appears most important for F100a in the receptor-binding site. Error bars indicate SD.

this study, and the RAVV GP was intact and uncleaved. However, a glycan cap was not visible. Instead, these 83 residues, their five predicted N-linked glycans, and four predicted O-linked glycans are disordered, and likely occupy the ~90 Å solvent channels between receptor-binding sites in the crystal packing. Marburgviruses and ebolaviruses possess little sequence identity in this region, and this domain of MARV GP is predicted to be more disordered than that of EBOV GP (Figure S2). These observations suggest that these residues of marburgvirus GP diverge structurally from the corresponding domain of ebolaviruses. A great many marburgvirus antibodies have been identified against the hydrophobic trough of the GP1, while no such antibodies are yet described for ebolaviruses, leading to speculation that this site is more exposed in marburgviruses than ebolaviruses. We note here, however, that NPC1-C is unable to bind uncleaved RAVV GP *in vitro* (Figure 4A). The RAVV glycan cap, although mobile in MR191- and MR78-bound structures, may still partially shield the receptor-binding site. The antibodies may simply better displace the cap than NPC1-C.

Interactions of mAb MR191 with RAVV GP

MR191 binds in the NPC1-C binding site of RAVV GP, interacting with both the hydrophobic trough and the crest at the apex of GP1 (Figures 3 and S4). CDRs H3, H2, L3, and L1 participate in this interaction. CDR H3 extends 11 Å into the hydrophobic trough of GP, with antibody residue F100a (Kabat numbering) at its apex interacting with W70, F72, and M154 of RAVV GP (residues equivalent to W86, F88, and I170 in EBOV GP). Along the C-terminal side of the extended CDR H3, residues V100b and W100d of MR191 form additional hydrophobic interactions with the pocket. Further, residue E100c of MR191 CDR H3 forms a hydrogen bond with Q128 of the crest of GP1, which rises above the hydrophobic trough. Four residues of CDR H2 (S52, S54, N56, and Y58) also hydrogen bond to Q128 and to

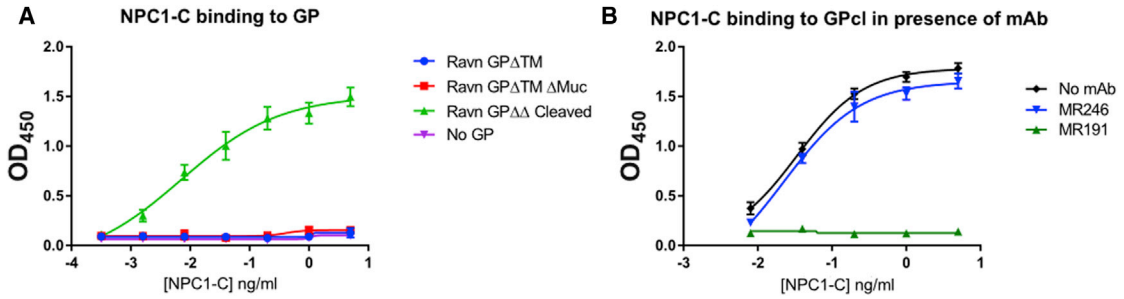

Figure 4. MR191 Outcompetes NPC1-C

(A) GP-coated plates were bound to antibody, blocked, and then incubated with HA-tagged NPC1-C in 5-fold dilutions. NPC1-C is unable to bind full-length or mucin-deleted RAVV GP ectodomain. It can, however, bind RAVV GP ectodomain from which the glycan cap is removed by limited proteolysis with trypsin.
(B) Competition of MR191 with NPC1-C demonstrated by ELISA. Negligible NPC1-C bound in the presence of MR191 (green). The non-competing mAb MR246, directed against another site on RAVV GP (Flyak et al., 2015), is shown as a control (blue).
Error bars indicate SD.

the main chain carbonyls of D99 and P100 of the GP1 crest (Figure 3). The light chain of MR191 forms a mixture of hydrophobic and hydrophilic contacts with the lower and outer rim of the GP trough.

Mimicry of, and Competition with, NPC1-C

MR191 mimics the interaction made by NPC1-C loop 2 in which an extended loop bearing a Phe (F100a in MR191, F131 in NPC1-C) at its apex binds into the GP hydrophobic trough (Wang et al., 2016). A Phe also is employed by the related human mAb MR78 (Hashiguchi et al., 2015), and by the EBOV and SUDV glycan caps, which insert into and mask this region prior to cathepsin cleavage (Lee et al., 2008; Dias et al., 2011; Bale et al., 2012; Zhao et al., 2016). An aromatic residue appears to be essential for interaction with this conserved filovirus site: mutation of F100a in the MR191 heavy chain to a tyrosine (F100aY) maintained binding to the GP, while mutation to an alanine (F100aA) greatly reduced the strength of the interaction (Figure 3C). Interestingly, however, the other strongly hydrophobic, aromatic residue inserted into the pocket, W100d, did not appear to be as critical for binding (Figure 3C). Based on their binding sites, it is perhaps unsurprising that MR191 outcompetes NPC1-C when assayed in a competition-binding ELISA (Figure 4). These results suggest that MR191 sterically interferes with the binding of NPC1-C as a primary mechanism of neutralization.

Mutagenesis and Binding

MR191 and NPC1-C appear to make similar interactions with the hydrophobic trough of filovirus GP, but only MR191 interacts with the crest (positioned above the receptor-binding site). We used mutagenesis to probe the antibody-GP interactions and determine which residues are critical for binding MR191 to marburgvirus GP.

In MR191, in addition to the mutants discussed above, we mutated two residues that interact with the hydrophilic rim around the trough (Y91 and T93 in CDR L3), and four residues that interact with the crest above (S52, S54, N56, and Y58 in CDR H2 and E100c in CDR H3). Notably, no single mutation to any residue that makes hydrophilic interactions, whether to the hydrophilic rim or crest, significantly affected binding: T93A and Y91A mutations in the light chain of MR191, and S54A, N56A, Y58A, and Y58F mutations in the heavy chain, each resulted in binding of GP equivalent to that of wild-type GP (Figure S3). In contrast, MR191 bearing an F100a to Ala point mutation exhibited a 225-fold increase in a half maximal effective concentration (EC_{50}) compared with that of wild-type MR191 binding (Figure 3). However, replacing F100a with a Tyr residue retained nearly equivalent levels of binding to that of the wild-type mAb. Mutation of the antibody residue W100d did not appear to affect the EC_{50} of binding.

In GP, we mutated five residues individually, F72A or W70A in the hydrophobic trough, and H124S, Q128S, or N129S in the crest. We also created GP with a Q128S/N129S double mutation in the crest. Four of the five single-point mutant GPs did not fold well or express, supporting the intolerance of both the trough and crest in this conserved site to mutagenic substitution (Manicassamy et al., 2007). The only mutants of RAVV GP that did express successfully were GPs with Q128S or Q128S/N129S substitutions. Q128S bound MR191 with a 2.5-fold increase in EC_{50} compared with wild-type, suggesting that interaction of the antibody with this basic crest is important (Figure S3). This interaction is unique to MR191 and is not made by NPC1-C.

Comparing MR191 to the Less Protective MR82 and MR78 Antibodies

MR191 was found to be more protective than MR82 or MR78 after marburgvirus challenge of guinea pigs (Mire et al., 2017). All three antibodies are contained in the same competition-binding group for interaction with GP, and all three recognize the NPC1-C binding site (Flyak et al., 2015; Hashiguchi et al., 2015). Notably, each of these three antibodies failed to neutralize the escape mutant viruses selected with either of the other two mAbs (Flyak et al., 2015). We sought to determine if there was a functional difference among the mAbs that could be measured *in vitro* and explain differences in level of *in vivo* protection. All three antibodies displayed similar ability to activate human natural killer or dendritic cells and macrophage- or neutrophil-mediated phagocytosis when bound to marburgvirus GP trimers (Figure S1). One difference noticed structurally between MR191 and MR78's binding

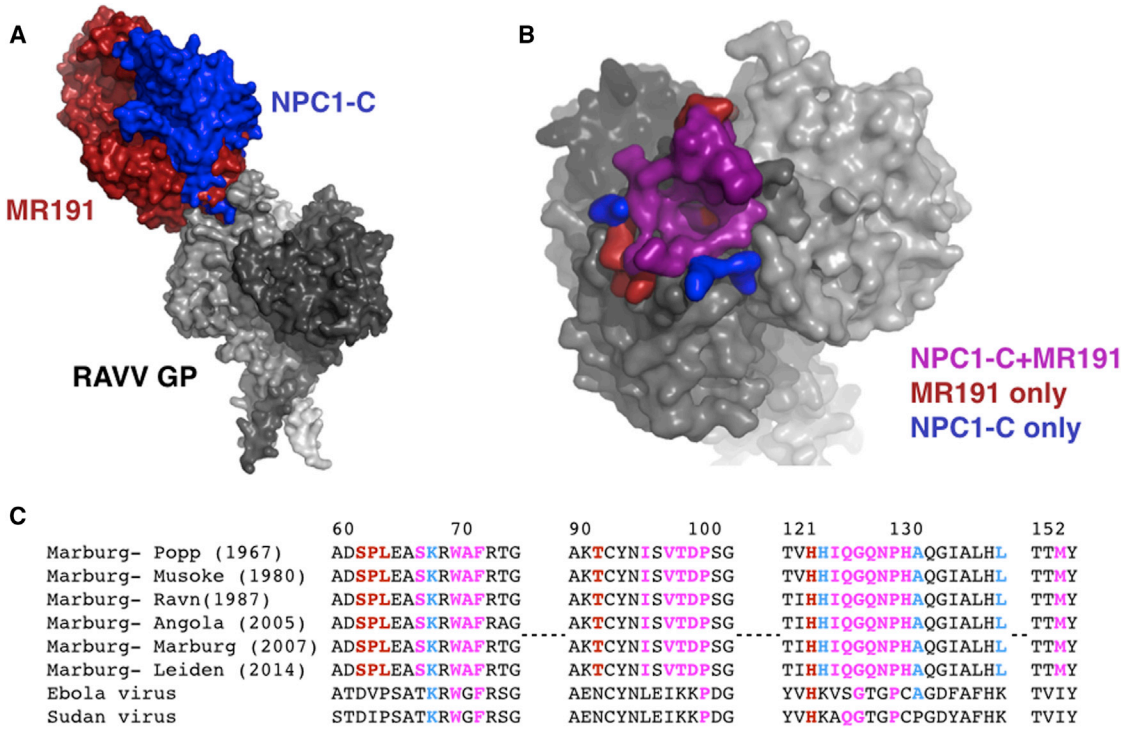

Figure 5. Overlapping Footprints of MR191 and NPC1-C

(A) Superimposed view of MR191 Fab/RAVV GP and NPC1-C/EBOV GP (PDB: 5F1B) (Wang et al., 2016) complexes. Only RAVV GP is illustrated for clarity.

(B) Corresponding footprints of MR191 and NPC1-C overlaid on the RAVV GP trimer and colored as in (A) to illustrate overlap between NPC1-C and MR191.

(C) Sequence alignment across historic and modern isolates of marburgvirus. Residues are colored as in (A) with MR191 only contacts in red, NPC1-C only contacts (for EBOV) in blue and shared contacts in purple. Contact residues are highly conserved among marburgviruses. Some residues are also conserved with EBOV and SUDV.

modality is that MR191 coordinates the crest of GP much more thoroughly; however, the importance of this interaction is unclear. Some other factor measurable *in vivo*, such as improved pharmacokinetics or biodistribution, may be responsible for the apparent superiority of MR191.

MR191 Escape Mutant Viruses

Structural modeling suggested that the footprints of MR191 and NPC1-C on marburgvirus GP overlap significantly, and the residues contacted by each are absolutely conserved in all marburgvirus isolates sequenced to date (Figure 5). To identify potential locations of variant GP residues that could mediate escape from recognition by MR191, we selected and analyzed antibody-resistant GP proteins. A chimeric vesicular stomatitis virus (VSV) displaying MARV GP was incubated with serial 2-fold dilutions of MR191 in nine independent replicate experiments (Flyak et al., 2015). Antibody-resistant virus suspensions were collected and the nucleotide sequence of GP ORF was determined. MR191-resistant VSV-GP viruses were identified in only three replicates, and were more difficult to isolate than for MR72 and MR78 (Flyak et al., 2015). Notably, when escape mutations were identified for MR191, they were not in the receptor-binding site footprint, but instead in the region corresponding to the glycan cap and the GP2 wing. The fact that escape only arises with substitution in distant, flexible locations suggests that these mutations may enhance occlusion of the receptor-binding site or have another effect on the quaternary structure.

DISCUSSION

This 3.2 Å crystal structure illuminates previously disordered regions of RAVV GP, including the IFL, the CX_6CC switch region of GP2, and the HR2 stalk below the GP base, as well as the anchor point of the marburgvirus-specific GP2 wing, one of two known protective antibody epitopes for marburgvirus. Unexpectedly, the RAVV GP2 wing anchor was found to wrap about the GP core, in place of the N terminus of GP1, which binds there in all ebolavirus GP structures. A further difference between marburgvirus and ebolavirus is that, although the RAVV GP crystallized contains residues in a similar primary sequence region to that of the ebolavirus glycan cap, none of these residues are visible in the structure.

These structural disparities between marburgviruses and ebolaviruses likely explain the differences in antibody reactivity and neutralization. Antibodies against the hydrophobic receptor-binding site constitute the majority of known neutralizing antibodies elicited by marburgvirus described thus far (Flyak et al., 2015; Hashiguchi et al., 2015), but no such antibodies are yet known to be elicited by ebolaviruses. Further, although MR191 binds both MARV GPcl and EBOV GPcl, as well as full-length MARV GP, it cannot bind or neutralize full-length EBOV GP,

suggesting that the ebolavirus glycan cap more effectively occludes the receptor-binding trough from antibody recognition than does the marburgvirus glycan cap (Brecher et al., 2012; Flyak et al., 2015). Further, numerous antibodies are known against the base of ebolavirus GP, such as KZ52, 2G4, 4G7, and mAb 114 (Lee et al., 2008; Dias et al., 2011; Murin et al., 2014; Misasi et al., 2016), but no such antibodies have been described for marburgviruses. The marburgvirus "base" equivalent may be occluded or partially occluded by the marburgvirus-specific wing epitope (Fusco et al., 2015).

MVD and EVD have significant outbreak potential, but lack any licensed therapeutics. Antibodies against these viruses may be used for emergency immunotherapy and in design of improved vaccines. MR191 is the only antibody yet demonstrated to confer complete protection to non-human primates after symptoms of MVD have developed, as late as 5 days after challenge (Mire et al., 2017). A principal concern with use of an antibody monotherapy, however, is the generation of viral escape mutants. MR191 engages the receptor-binding site of marburgvirus GP with CDR H3, mimicking the binding mode of NPC1-C (Figure 3), and with a footprint that overlaps dramatically with that of NPC1-C (Figure 5). All residues that MR191 contacts in GP are conserved among marburgviruses, with no single divergent mutant present in any strain yet sequenced since its original discovery in 1967 (Figure 5). Further, MR191 also binds EBOV GPcl (Bornholdt et al., 2016; Flyak et al., 2015), which is ~70% different in primary sequence from RAVV in the MR191 footprint residues. MR191 thus appears somewhat tolerant of substitution in its footprint and may be more resistant to escape than single antibodies against other sites. Further, most mutations made to residues in its receptor-binding site footprint result in poorly folded, poorly expressed GP, and/or non-rescuable viruses (Manicassamy et al., 2007). Hence, while MR191 tolerates substitution in its paratope, RAVV GP seems intolerant of substitution in the MR191 epitope.

Here, however, we note that escape mutations, derived from mAb selections using the chimeric VSV, could be generated in areas distant from the receptor-binding site, in the glycan cap equivalent and in the GP2 wing, consistent with previous observations (Flyak et al., 2015). Interestingly, these mutations suggest an as-yet unexplored mechanism by which the disordered regions of GP1 and GP2 influence viral entry or the quaternary structure of GP. It is unknown if such mutations would arise *in vivo;* escape mutations were not identified in non-human primates treated with MR191 (Mire et al., 2017).

The importance of the receptor-binding site to viral entry, the *in vivo* performance of the antibody in non-human primates, and the conservation and relative resistance of the site to substitution suggests that MR191 is an appropriate first immunotherapeutic for development against MVD. Cocktails could be formulated when antibodies against other marburgvirus GP epitopes show success in non-human primates.

STAR★METHODS

Detailed methods are provided in the online version of this paper and include the following:

- KEY RESOURCES TABLE
- CONTACT FOR REAGENT AND RESOURCE SHARING
- EXPERIMENTAL MODEL AND SUBJECT DETAILS
  - Plant Strains
  - Cells
- METHOD DETAILS
  - Construction, Expression and Purification of RAVV GP and MR191
  - Preparation and Crystallization of GP-Antibody Complex
  - X-ray Data Collection and Experimental Structure Determination
  - Rosetta Modeling of the MR191-RAVV GP Complex and Phenix.Rosetta Refinement
  - ELISA Evaluation of MR191 Mutants
  - Effector Function Studies
- QUANTIFICATION AND STATISTICAL ANALYSIS
- DATA AND SOFTWARE AVAILABILITY

SUPPLEMENTAL INFORMATION

Supplemental Information includes five figures and two tables and can be found with this article online at https://doi.org/10.1016/j.chom.2017.12.003.

ACKNOWLEDGMENTS

We thank Drs. Zachary Bornholdt and Larry Zeitlin of Mapp Biopharmaceutical for the gift of MR191, MR82, and MR78 IgG and for helpful discussions. R01AI089498 and U19AI109762 (E.O.S.), U19AI109762 (G.A.), HDTRA1-13-1-0034 (J.E.C.), NIH 1U19AI109711 (J.E.C. and A.B.), and R21AI121799 (J.M.) provided financial support. We thank the staff of beamline 23-ID-D of the Advanced Photon Source and beamline 12-2 of the Stanford Synchrotron Radiation Lightsource for assistance with data collection. This research used resources of the Advanced Photon Source, a U.S. Department of Energy (DOE) Office of Science User Facility operated for the DOE Office of Science by Argonne National Laboratory under Contract no. DE-AC02-06CH11357. Use of the Stanford Synchrotron Radiation Lightsource, SLAC National Accelerator Laboratory, is supported by the U.S. Department of Energy, Office of Science, Office of Basic Energy Sciences under Contract no. DE-AC02-76SF00515. The SSRL Structural Molecular Biology Program is supported by the DOE Office of Biological and Environmental Research and by the NIH, National Institute of General Medical Sciences (including P41GM103393). Coordinates and structure factors for the MR191-RAVV GP complex have been deposited into the Protein Data Bank under accession number PDB: 6BP2. In light of the higher-resolution map described here, the earlier model of RAVV GP (PDB: 3X2D) has been updated and is available at PDB: 5UQY. This is manuscript number 29544 from The Scripps Research Institute.

AUTHOR CONTRIBUTIONS

Conceptualization, L.B.K., M.L.F., A.B., J.E.C., and E.O.S.; Methodology, L.B.K., M.L.F., B.G., R.N.K., and A.K.S.; Validation, R.N.K. and K.M.H.; Investigation, L.B.K., M.L.F., A.I.F., P.A.I., K.H., B.G., and A.K.S.; Resources, J.E.C. and E.O.S.; Writing – Original Draft, L.B.K. and E.O.S.; Writing – Review & Editing, all authors; Visualization, L.B.K. and E.O.S.; Supervision, J.M., G.A., A.B., J.E.C., and E.O.S.; Project Administration, J.E.C., A.B., and E.O.S.; Funding Acquisition, J.M., G.A., A.B., J.E.C., and E.O.S.

DECLARATION OF INTERESTS

J.E.C., A.B., A.I.F., and P.A.I. are listed as co-inventors for a patent submitted, which includes in part claims relating to MR191. The MR191 antibody has been licensed by Vanderbilt University to a commercial partner.

Received: July 31, 2017
Revised: October 28, 2017
Accepted: December 8, 2017
Published: January 10, 2018

REFERENCES

Adams, P.D., Afonine, P.V., Bunkóczi, G., Chen, V.B., Davis, I.W., Echols, N., Headd, J.J., Hung, L.W., Kapral, G.J., Grosse-Kunstleve, R.W., et al. (2010). PHENIX: a comprehensive Python-based system for macromolecular structure solution. Acta Crystallogr. D Biol. Crystallogr. *66* (Pt 2), 213–221.

Aleksandrowicz, P., Marzi, A., Biedenkopf, N., Beimforde, N., Becker, S., Hoenen, T., Feldmann, H., and Schnittler, H.J. (2011). Ebola virus enters host cells by macropinocytosis and clathrin-mediated endocytosis. J. Infect. Dis. *204* (*Suppl 3*), S957–S967.

Altschul, S.F., Gish, W., Miller, W., Myers, E.W., and Lipman, D.J. (1990). Basic local alignment search tool. J. Mol. Biol. *215*, 403–410.

Bale, S., Dias, J.M., Fusco, M.L., Hashiguchi, T., Wong, A.C., Liu, T., Keuhne, A.I., Li, S., Woods, V.L., Jr., Chandran, K., et al. (2012). Structural basis for differential neutralization of ebolaviruses. Viruses *4*, 447–470.

Bendandi, M., Marillonnet, S., Kandzia, R., Thieme, F., Nickstadt, A., Herz, S., Fröde, R., Inogés, S., Lòpez-Dìaz de Cerio, A., Soria, E., et al. (2010). Rapid, high-yield production in plants of individualized idiotype vaccines for non-Hodgkin's lymphoma. Ann. Oncol. *21*, 2420–2427.

Bender, B.J., Cisneros, A., 3rd, Duran, A.M., Finn, J.A., Fu, D., Lokits, A.D., Mueller, B.K., Sangha, A.K., Sauer, M.F., Sevy, A.M., et al. (2016). Protocols for molecular modeling with Rosetta3 and RosettaScripts. Biochem *55*, 4748–4763.

Bornholdt, Z.A., Ndungo, E., Fusco, M.L., Bale, S., Flyak, A.I., Crowe, J.E., Jr., Chandran, K., and Saphire, E.O. (2016). Host-primed Ebola virus GP exposes a hydrophobic NPC1 receptor-binding pocket, revealing a target for broadly neutralizing antibodies. MBio *7*, https://doi.org/10.1128/mBio.02154-15.

Brecher, M., Schornberg, K.L., Delos, S.E., Fusco, M.L., Saphire, E.O., and White, J.M. (2012). Cathepsin cleavage potentiates the Ebola virus glycoprotein to undergo a subsequent fusion-relevant conformational change. J. Virol. *86*, 364–372.

Bricogne, G. (1993). Direct phase determination by entropy maximization and likelihood ranking: status report and perspectives. Acta Crystallogr. D Biol. Crystallogr. *49* (Pt 1), 37–60.

Bukreyev, A., Volchkov, V.E., Blinov, V.M., and Netesov, S.V. (1993). The GP-protein of Marburg virus contains the region similar to the 'immunosuppressive domain' of oncogenic retrovirus P15E proteins. FEBS Lett. *323*, 183–187.

Burton, D.R., and Saphire, E.O. (2015). Swift antibodies to counter emerging viruses. Proc. Natl. Acad. Sci. USA *112*, 10082–10083.

Carette, J.E., Raaben, M., Wong, A.C., Herbert, A.S., Obernosterer, G., Mulherkar, N., Kuehne, A.I., Kranzusch, P.J., Griffin, A.M., Ruthel, G., et al. (2011). Ebola virus entry requires the cholesterol transporter Niemann-Pick C1. Nature *477*, 340–343.

CDC. (2005). Brief report: outbreak of Marburg virus hemorrhagic fever –- Angola. October 1, 2004 – March 29, 2005. CDC. Available at: http://www.cdc.gov/mmwr/preview/mmwrhtml/mm54d330a1.htm.

Chandran, K., Sullivan, N.J., Felbor, U., Whelan, S.P., and Cunningham, J.M. (2005). Endosomal proteolysis of the Ebola virus glycoprotein is necessary for infection. Science *308*, 1643–1645.

Chanock, R.M., Crowe, J.E., Jr., Murphy, B.R., and Burton, D.R. (1993). Human monoclonal antibody Fab fragments cloned from combinatorial libraries: potential usefulness in prevention and/or treatment of major human viral diseases. Infect. Agent Dis. *2*, 118–131.

Chen, V.B., Arendall, W.B., 3rd, Headd, J.J., Keedy, D.A., Immormino, R.M., Kapral, G.J., Murray, L.W., Richardson, J.S., and Richardson, D.C. (2010). MolProbity: all-atom structure validation for macromolecular crystallography. Acta Crystallogr. D Biol. Crystallogr. *66* (Pt 1), 12–21.

Dias, J.M., Kuehne, A.I., Abelson, D.M., Bale, S., Wong, A.C., Halfmann, P., Muhammad, M.A., Fusco, M.L., Zak, S.E., Kang, E., et al. (2011). A shared structural solution for neutralizing ebolaviruses. Nat. Struct. Mol. Biol. *18*, 1424–1427.

DiMaio, F., Echols, N., Headd, J.J., Terwilliger, T.C., Adams, P.D., and Baker, D. (2013). Improved low-resolution crystallographic refinement with Phenix and Rosetta. Nat. Methods *10*, 1102–1104.

Dye, J.M., Herbert, A.S., Kuehne, A.I., Barth, J.F., Muhammad, M.A., Zak, S.E., Ortiz, R.A., Prugar, L.I., and Pratt, W.D. (2012). Postexposure antibody prophylaxis protects nonhuman primates from filovirus disease. Proc. Natl. Acad. Sci. USA *109*, 5034–5039.

Emsley, P., and Cowtan, K. (2004). Coot: model-building tools for molecular graphics. Acta Crystallogr. D Biol. Crystallogr. *60* (Pt 12 Pt 1), 2126–2132.

Feldmann, H., Klenk, H.D., and Sanchez, A. (1993). Molecular biology and evolution of filoviruses. Arch. Virol. Suppl. *7*, 81–100.

Finn, J.A., Koehler Leman, J., Willis, J.R., Cisneros, A., 3rd, Crowe, J.E., Jr., and Meiler, J. (2016). Improving loop modeling of the antibody complementarity-determining region 3 using knowledge-based restraints. PLoS One *11*, e0154811.

Flyak, A.I., Ilinykh, P.A., Murin, C.D., Garron, T., Shen, X., Fusco, M.L., Hashiguchi, T., Bornholdt, Z.A., Slaughter, J.C., Sapparapu, G., et al. (2015). Mechanism of human antibody-mediated neutralization of Marburg virus. Cell *160*, 893–903.

Fusco, M.L., Hashiguchi, T., Cassan, R., Biggins, J.E., Murin, C.D., Warfield, K.L., Li, S., Holtsberg, F.W., Shulenin, S., Vu, H., et al. (2015). Protective mAbs and cross-reactive mAbs raised by immunization with engineered Marburg virus GPs. PLoS Pathog. *11*, e1005016.

Gnirss, K., Kühl, A., Karsten, C., Glowacka, I., Bertram, S., Kaup, F., Hofmann, H., and Pöhlmann, S. (2012). Cathepsins B and L activate Ebola but not Marburg virus glycoproteins for efficient entry into cell lines and macrophages independent of TMPRSS2 expression. Virology *424*, 3–10.

Gong, X., Qian, H., Zhou, X., Wu, J., Wan, T., Cao, P., Huang, W., Zhao, X., Wang, X., Wang, P., et al. (2016). Structural insights into the Niemann-Pick C1 (NPC1)-mediated cholesterol transfer and Ebola infection. Cell *165*, 1467–1478.

PREVAIL II Writing Group; Multi-National PREVAIL II Study Team, Davey, R.T., Jr., Dodd, L., Proschan, M.A., Neaton, J., Neuhaus Nordwall, J., Koopmeiners, J.S., Beigel, J., and Tierney, J. (2016). A randomized, controlled trial of ZMapp for Ebola virus infection. N. Engl. J. Med. *375*, 1448–1456.

Hashiguchi, T., Fusco, M.L., Bornholdt, Z.A., Lee, J.E., Flyak, A.I., Matsuoka, R., Kohda, D., Yanagi, Y., Hammel, M., Crowe, J.E., Jr., et al. (2015). Structural basis for Marburg virus neutralization by a cross-reactive human antibody. Cell *160*, 904–912.

Hood, C.L., Abraham, J., Boyington, J.C., Leung, K., Kwong, P.D., and Nabel, G.J. (2010). Biochemical and structural characterization of cathepsin L-processed Ebola virus glycoprotein: implications for viral entry and immunogenicity. J. Virol. *84*, 2972–2982.

Kabsch, W. (2010). Integration, scaling, space-group assignment and post-refinement. Acta Crystallogr. D Biol. Crystallogr. *66* (Pt 2), 133–144.

Kaufmann, K.W., Lemmon, G.H., Deluca, S.L., Sheehan, J.H., and Meiler, J. (2010). Practically useful: what the Rosetta protein modeling suite can do for you. Biochemistry *49*, 2987–2998.

Lachmann, P.J. (2012). The use of antibodies in the prophylaxis and treatment of infections. Emerg. Microbes Infect. *1*, e11.

Lee, J.E., Fusco, M.L., Hessell, A.J., Oswald, W.B., Burton, D.R., and Saphire, E.O. (2008). Structure of the Ebola virus glycoprotein bound to an antibody from a human survivor. Nature *454*, 177–182.

Manicassamy, B., Wang, J., Rumschlag, E., Tymen, S., Volchkova, V., Volchkov, V., and Rong, L. (2007). Characterization of Marburg virus glycoprotein in viral entry. Virology *358*, 79–88.

Marillonnet, S., Thoeringer, C., Kandzia, R., Klimyuk, V., and Gleba, Y. (2005). Systemic *Agrobacterium tumefaciens*-mediated transfection of viral replicons for efficient transient expression in plants. Nat. Biotechnol. *23*, 718–723.

Marzi, A., Reinheckel, T., and Feldmann, H. (2012). Cathepsin B & L are not required for Ebola virus replication. PLoS Negl. Trop. Dis. *6*, e1923.

McCoy, A.J., Grosse-Kunstleve, R.W., Adams, P.D., Winn, M.D., Storoni, L.C., and Read, R.J. (2007). Phaser crystallographic software. J. Appl. Crystallogr. *40* (Pt 4), 658–674.

Miller, E.H., Obernosterer, G., Raaben, M., Herbert, A.S., Deffieu, M.S., Krishnan, A., Ndungo, E., Sandesara, R.G., Carette, J.E., Kuehne, A.I., et al.

(2012). Ebola virus entry requires the host-programmed recognition of an intracellular receptor. EMBO J. *31*, 1947–1960.

Mire, C.E., Geisbert, J.B., Borisevich, V., Fenton, K.A., Agans, K.N., Flyak, A.I., Deer, D.J., Steinkellner, H., Bohorov, O., Bohorova, N., et al. (2017). Therapeutic treatment of Marburg and Ravn virus infection in nonhuman primates with a human monoclonal antibody. Sci. Transl. Med. *9*, https://doi.org/10.1126/scitranslmed.aai8711.

Misasi, J., Gilman, M.S., Kanekiyo, M., Gui, M., Cagigi, A., Mulangu, S., Corti, D., Ledgerwood, J.E., Lanzavecchia, A., Cunningham, J., et al. (2016). Structural and molecular basis for Ebola virus neutralization by protective human antibodies. Science *351*, 1343–1346.

Mulherkar, N., Raaben, M., de la Torre, J.C., Whelan, S.P., and Chandran, K. (2011). The Ebola virus glycoprotein mediates entry via a non-classical dynamin-dependent macropinocytic pathway. J. Virol. *419*, 72–83.

Murin, C.D., Fusco, M.L., Bornholdt, Z.A., Qiu, X., Olinger, G.G., Zeitlin, L., Kobinger, G.P., Ward, A.B., and Saphire, E.O. (2014). Structures of protective antibodies reveal sites of vulnerability on Ebola virus. Proc. Natl. Acad. Sci. USA *111*, 17182–17187.

Nanbo, A., Imai, M., Watanabe, S., Noda, T., Takahashi, K., Neumann, G., Halfmann, P., and Kawaoka, Y. (2010). Ebolavirus is internalized into host cells via macropinocytosis in a viral glycoprotein-dependent manner. PLoS Pathog. *6*, e1001121.

Olinger, G.G., Jr., Pettitt, J., Kim, D., Working, C., Bohorov, O., Bratcher, B., Hiatt, E., Hume, S.D., Johnson, A.K., Morton, J., et al. (2012). Delayed treatment of Ebola virus infection with plant-derived monoclonal antibodies provides protection in rhesus macaques. Proc. Natl. Acad. Sci. USA *109*, 18030–18035.

Pallesen, J., Murin, C.D., de Val, N., Cottrell, C.A., Hastie, K.M., Turner, H.L., Fusco, M.L., Flyak, A.I., Zeitlin, L., Crowe, J.E., Jr., et al. (2016). Structures of Ebola virus GP and sGP in complex with therapeutic antibodies. Nat. Microbiol. *1*, 16128.

Qiu, X., Wong, G., Audet, J., Bello, A., Fernando, L., Alimonti, J.B., Fausther-Bovendo, H., Wei, H., Aviles, J., Hiatt, E., et al. (2014). Reversion of advanced Ebola virus disease in nonhuman primates with ZMapp. Nature *514*, 47–53.

Saeed, M.F., Kolokoltsov, A.A., Albrecht, T., and Davey, R.A. (2010). Cellular entry of Ebola virus involves uptake by a macropinocytosis-like mechanism and subsequent trafficking through early and late endosomes. PLoS Pathog. *6*, e1001110.

Schornberg, K., Matsuyama, S., Kabsch, K., Delos, S., Bouton, A., and White, J. (2006). Role of endosomal cathepsins in entry mediated by the Ebola virus glycoprotein. J. Virol. *80*, 4174–4178.

Song, Y., DiMaio, F., Wang, R.Y., Kim, D., Miles, C., Brunette, T., Thompson, J., and Baker, D. (2013). High-resolution comparative modeling with RosettaCM. Structure *21*, 1735–1742.

Volchkov, V.E., Feldmann, H., Volchkova, V.A., and Klenk, H.D. (1998). Processing of the Ebola virus glycoprotein by the proprotein convertase furin. Proc. Natl. Acad. Sci. USA *95*, 5762–5767.

Volchkov, V.E., Volchkova, V.A., Ströher, U., Becker, S., Dolnik, O., Cieplik, M., Garten, W., Klenk, H.D., and Feldmann, H. (2000). Proteolytic processing of Marburg virus glycoprotein. Virology *268*, 1–6.

Wang, H., Shi, Y., Song, J., Qi, J., Lu, G., Yan, J., and Gao, G.F. (2016). Ebola viral glycoprotein bound to its endosomal receptor Niemann-Pick C1. Cell *164*, 258–268.

Zeitlin, L., Cone, R.A., and Whaley, K.J. (1999). Using monoclonal antibodies to prevent mucosal transmission of epidemic infectious diseases. Emerg. Infect. Dis. *5*, 54–64.

Zhao, Y., Ren, J., Harlos, K., and Stuart, D.I. (2016). Structure of glycosylated NPC1 luminal domain C reveals insights into NPC2 and Ebola virus interactions. FEBS Lett. *590*, 605–612.

STAR★METHODS

KEY RESOURCES TABLE

REAGENT or RESOURCE	SOURCE	IDENTIFIER
Antibodies		
MR191	Mapp Biopharmaceutical Inc.	
MR78	Mapp Biopharmaceutical Inc.	
MR82	Mapp Biopharmaceutical Inc.	
Mouse anti-human IgG1 Fc secondary antibody HRP	ThermoFisher Scientific	Cat #: A-10648 RRID: AB_2534051
Mouse anti-human CD66b (clone G10F5)	Biolegend	Cat#: 305112 RRID: AB_2563294
Mouse anti-human CD107a (clone H4A3)	BD Biosciences	Cat #: 555802 RRID:AB_396136
Mouse anti-human IFNg (clone B27)	BD Biosciences	Cat #: 554702 RRID:AB_398580
Mouse anti-human CD56 (clone B159)	BD Biosciences	Cat #: 557747 RRID:AB_396853
Mouse anti-human CD80 (clone L307.4)	BD Biosciences	Cat #: 561134 RRID:AB_10565974
Mouse anti-human CD86 (clone FUN-1)	BD Biosciences	Cat #: 561128 RRID:AB_10563077
Mouse anti-human CD14 (clone MφP9)	BD Biosciences	Cat# 560180 RRID:AB_1645464
Mouse anti-human CD16 (clone 3G8)	BD Biosciences	Cat #: 557758 RRID:AB_396864
Mouse anti-human CD3 (clone UCHT1)	BD Biosciences	Cat #: 557943 RRID:AB_396952
Mouse anti-human MIP-1b (clone D21-1351)	BD Biosciences	Cat #: 550078 RRID:AB_393549
Deposited Data		
RCSB Protein Data Bank		PDB: 6BP2
Experimental Models: Cell Lines		
Drosophila S2	Invitrogen	Cat# ACC-130, RRID:CVCL_Z232
FreeStyle 293-F	Thermo Fisher Scientific	Cat# PTA-5080, RRID:CVCL_D603
Human monocytes	ATCC	ATCC: PCS-800-010
Human neutrophils	Isolated from human donors	
Human monocyte-derived dendritic cells	Isolated from human donors	http://www.miltenyibiotec.com/en/products-and-services/macs-cell-separation/cell-separation-reagents/monocytes-and-macrophages/cd14-microbeads-human.aspx
Human natural killer cells	Isolated from human donors	ttps://www.stemcell.com/products/rosettesep-human-nk-cell-enrichment-cocktail.html#section-overview
Nicotiana benthamania strain delta XF	Kentucky Bioprocessing	Marillonnet et al., 2005
Agrobacterium tumefaciens strain ICF320		Bendandi et al., 2010
Recombinant DNA		
Ravn virus GP	Cangene	

(*Continued on next page*)

Continued

REAGENT or RESOURCE	SOURCE	IDENTIFIER
Software and Algorithms		
Phenix.refine	Adams et al., 2010	https://www.phenix-online.org/documentation/reference/refinement.html
BUSTER	Bricogne, 1993	https://www.globalphasing.com/buster/manual/autobuster/manual/index.html
XDS	Kabsch, 2010	http://xds.mpimf-heidelberg.mpg.de/html_doc/downloading.html
Phaser	McCoy et al., 2007	https://www.phenix-online.org/documentation/reference/phaser.html
MolProbity	Chen et al., 2010	http://molprobity.biochem.duke.edu/
COOT	Emsley and Cowtan, 2004	https://www2.mrc-lmb.cam.ac.uk/personal/pemsley/coot/
Phenix.rosetta_refine	DiMaio et al., 2013	https://www.rosettacommons.org
RosettaCM	Song et al., 2013	https://www.rosettacommons.org
RosettaDock	Kaufmann et al., 2010; Bender et al., 2016	https://www.rosettacommons.org

CONTACT FOR REAGENT AND RESOURCE SHARING

Correspondence should be directed to Erica Ollmann Saphire (erica@scripps.edu). Requests for MR191 and other antibodies should be directed to James E. Crowe, Jr. (james.crowe@vanderbilt.edu), which can be made available upon request through a Materials Transfer Agreement.

EXPERIMENTAL MODEL AND SUBJECT DETAILS

Plant Strains

Nicotiana benthamiana plants were grown for 24-26 d in an enclosed growth room at 22-24°C as described in Olinger et al., 2012 and below.

Cells

Stable lines were formed using *Drosophila* Schneider S2 cells grown in Schneider's *Drosophila* Medium at 27°C. S2 cells for protein expression were grown in Insect-XPRESS protein-free medium with L-glutamine (Lonza) supplemented with puromycin (6 μg/mL) (InvivoGen) at 27°C.

Vero-E6 cells for generation and analysis of chimeric VSV escape mutants were obtained from ATCC and maintained in Dulbecco Minimal Essential Medium (DMEM) (ThermoFisher Scientific) supplemented by 10% fetal bovine serum (HyClone) and 1% penicillin-streptomycin at 5% CO_2, 37°C.

METHOD DETAILS

Construction, Expression and Purification of RAVV GP and MR191

Ravn virus GPΔmuc (including residues 1-636, with 257-425 deleted to remove the mucin-like domain) was expressed in *Drosophila* Schneider S2 cells. GP was collected by StepTactin affinity purification (GE Healthcare Life Sciences). Removal of the double Strep tag at the enterokinase cleavage site improved crystallization and was achieved by incubation of RAVV GPΔmuc with enterokinase (Invitrogen) at 2.5 U/mg of glycoprotein at 4°C overnight followed by passage through on a StrepTactin affinity column.

Hybridoma cells expressing human MR191 IgG were generated previously from peripheral blood mononuclear cells (PBMCs) from a donor who contracted MARV infection while visiting the Python Cave in Queen Elizabeth National Park, Uganda in 2008 (Flyak et al., 2015). For larger scale production of mAbs MR191, MR78, and MR82, the variable region sequences were used as reported and codon optimized. Genes containing these sequences were synthesized (Life Technologies) and subsequently cloned into plant expression vectors (TMV and PVX, Icon Genetics, GmbH) containing codon-optimized human constant regions followed by transformation into *Agrobacterium tumefaciens* strain ICF320 (Bendandi et al., 2010).

We used the "magnifection" procedure (Marillonnet et al., 2005) with minor modifications for production of mAb. Plants grown for 4 weeks in an enclosed growth room (20-23°C) were used for vacuum infiltration. Equal volumes of Agrobacterium cultures grown overnight were mixed in infiltration buffer (1 mM MES/10 mM MgSO4, pH 5.5), resulting in a 1:1000 dilution for each individual culture. Infiltration solution was transferred into a 20 L custom built (Kentucky Bioprocessing) vacuum chamber. The aerial parts of the plants were inverted into the bacterial/buffer solution. A vacuum of 0.5 bars was applied for 2 min, and the plants were returned to the growth room. Seven days post-infiltration, leaf tissue was extracted in a juicer (Model GS-1000, Green Star) using 250 mL of chilled extraction buffer (100 mM Tris/40 mM ascorbic acid/1 mM EDTA) per kg of green leaf tissue. The extract was clarified by lowering

the pH to 4.8 with 1 M phosphoric acid then re-adjusting to pH 7.5 with 2 M Tris base to insolubilize the plant polymers. The supernatant was transferred and centrifuged at 16,000 x g for 30 min. The clarified extract was filtered (0.2 μm) prior to concentration using the Minim Tangential Flow Filtration System (Pall) and then 0.2 μm was filtered immediately prior to loading onto a 5 mL HiTrap MabSelect SuRe (GE Healthcare Life Sciences) Protein A column at 2 mL/min. The column was washed with running buffer (50 mM HEPES/100 mM NaCl, pH 7.5) and eluted with 0.1 M acetic acid, pH 3.0. The resulting eluate was neutralized to pH 7 using 2 M Tris, pH 8.0, and ╲emented with Tween 80 to 0.01%. The IgG containing solution was polished via Q filtration (Mustang Acrodisc Q membrane, Pall), aliquoted, and stored at -80°C until use. Fab fragments were generated from purified IgG using 4% w/w papain digestion for 6 hr, followed by Mono Q anion exchange chromatography (GE Healthcare Life Sciences), and size exclusion chromatography (GE Healthcare Life Sciences).

Preparation and Crystallization of GP-Antibody Complex

For crystallization, purified RAVV GPΔmuc was mixed with a 10-fold excess of MR191 Fab overnight at room temperature. Complexes were separated from unbound antibody and GP via size-exclusion chromatography on Superdex 200 (GE Healthcare Life Sciences) resin. Crystals were grown via sitting-drop vapor diffusion at room temperature using 0.2 μl of protein (7.0 mg/ml, in 10 mM Tris-HCl (pH 7.5), 100 mM NaCl) and 0.2 μl of mother liquor (100 mM HEPES pH 7.5, 5% PEG 3000, 26% PEG 400, 6% Glycerol). Crystals were harvested and flash-cooled immediately in liquid nitrogen without additional cryoprotectant.

X-ray Data Collection and Experimental Structure Determination

Single-crystal X-ray diffraction data for the RAVV GP-MR191 Fab complex were collected at beamline 23-ID-D (using a Dectris PILATUS3 6M detector) of the Advanced Photon Source (Argonne National Labs, United States). Images were processed and scaled using XDS (Kabsch, 2010). The initial model was determined by molecular replacement in Phaser (McCoy et al., 2007) using the separate molecules of RAVV GPcl and the Fab fragment from PDB ID: 3X2D (Hashiguchi et al., 2015) as search models. Further model refinement procedures were carried out using Phenix.refine (Adams et al., 2010) and BUSTER software (Bricogne, 1993). Iterative manual model building and correction were performed using COOT (Emsley and Cowtan, 2004). Models constructed using RosettaCM (see below) were used in structure determination of loops. The final structure was refined to R_{work} and R_{free} of 26.3 and 29.1 respectively, with a root mean square deviation of 0.012 in bond lengths and 1.520 in bond angles. Phenix.rosetta_refine (DiMaio et al., 2013) was used to select rotamers for several ambiguous residues. The quality of the final model was examined using MolProbity (Chen et al., 2010) and simulated annealing composite omit maps generated in Phenix (Adams et al., 2010). The final structure has been deposited to the RCSB Protein Data Bank under ID code 6BP2.

Rosetta Modeling of the MR191-RAVV GP Complex and Phenix.Rosetta Refinement

MR191 modeling and docking studies were performed to assist experimental X-ray structure determination. Unbound MR191 was first modeled by aligning its sequence to known antibody structures using PSIBLAST (Altschul et al., 1990) and comparative modeling was done using RosettaCM (Song et al., 2013). Torsional angle restraints were applied in RosettaCM to remodel the CDR-H3 (Finn et al., 2016). Nine models of MR191, selected for representation of the most significant clusters and lowest energy scores, were docked onto RAVV GP using RosettaDock (Kaufmann et al., 2010; Bender et al., 2016), as rigid bodies allowing a 3 Å translation and 8° rotation to antibody, while keeping GP fixed. Conformational space was constrained by pre-orienting MR191 to the receptor-binding site using observations from electron microscopy (EM). Four of nine potential complex orientations were pursued after relaxation into EM density. For each of the four docking sets, 1,000 models were generated and analyzed for Rosetta total score and binding energy. The CDR conformations from the two lowest energy models assisted in manual structure refinement into the crystallographic data. This procedure was particularly useful in construction of CDR L1 into electron density.

The best-scoring computationally docked complex, however, has MR191 oriented at a different angle than is observed in the crystal structure. This might be due to deviations in the conformation of CDR H3 between the Rosetta model and crystal structure (Figure S4). The Phenix.Rosetta protocol in Rosetta was run on the manually refined MR191-RAVV GP complex structure to predict side chain rotamers that were ambiguous. The low_resolution_refine.xml script (available in Rosetta/main/source/src/apps/public/crystal_refinement) was used with default parameters and talaris2013 score function (DiMaio et al., 2013).

ELISA Evaluation of MR191 Mutants

The genes encoding MR191 variable regions were synthesized and cloned into a mammalian IgG expression plasmid vector by GenScript Site-directed mutagenesis was performed using QuikChange Lightning Site-Directed Mutagenesis kit (Agilent). Transient expression of MR191 variants was done in Freestyle 293-F cells (Thermo Fisher Scientific). MAbs were harvested from filtered supernatants using HiTrap MabSelectSure columns (Life Technologies). ELISA plates were coated with *Drosophila* S2 cell-expressed Marburgvirus Ravn GPΔmuc at 4 ng/μl. Wild-type or point mutant MR191 were incubated at 25 μg/ml with six subsequent 10-fold dilutions. Binding was detected with HRP-conjugated anti-human Fc secondary antibodies (Thermo Fischer Scientific), and absorbance was measured using a TECAN Spark 10M. Results were analyzed and EC_{50} values calculated using GraphPad Prism software.

Effector Function Studies

NK Cell Activation and Degranulation

3 μg/ml of recombinant, trimeric RAVV GP was coated on a Maxisorp ELISA plate. Plates were blocked with 5% BSA prior to addition of antibodies MR191, MR78, or MR82 (range of concentration 5 μg/ml to 0.1 μg/ml) for 2 hr at 37°C. Human NK cells were enriched from donor peripheral blood by negative selection using RosetteSep (Stem Cell Technologies) followed by ficoll separation and were incubated with IL-15 (1 ng/ml) overnight at 37°C. The antibodies were removed and the wells washed prior to addition of NK cells. The NK cells were added at 2.5 x 10^4 cells/well in the presence of brefeldin A (Sigma Aldrich), GolgiStop (BD), and anti-CD107a and incubated for 5 hr at 37°C. NK cells were stained for surface markers of NK cells (CD3, CD56, CD16, BD Biosciences), and then stained intracellularly for the production of cytokines and chemokines (IFNγ and MIP-1β, BD Biosciences). Cells were analyzed by flow cytometry on an LSR II flow cytometer (BD Biosciences), and the resulting data were analyzed using FlowJo software.

Antibody-Mediated Cellular Phagocytosis by Human Monocytes

RAVV GP was biotinylated and conjugated to streptavidin-coated Alexa488 beads (Life Technologies). Antibodies (range of concentration 5 μg/ml to 0.1 μg/ml) were incubated with beads for 2 hr at 37°C. Human monocytic cells (THP-1) were added at a concentration of 2.5 x 10^4 cells/well and incubated for approximately 18 hr at 37°C. Cells were fixed and analyzed by flow cytometry and a phagocytic score was determined using the percentage of $FITC^+$ cells and the mean fluorescent intensity (MFI) of the FITC+ cells.

Antibody-Mediated Neutrophil Phagocytosis

RAVV GP was biotinylated and conjugated to streptavidin-coated Alexa488 beads. mAbs (range of concentration 5 μg/ml to 0.1 μg/ml) were incubated with beads for 2 hr at 37°C. Human neutrophils freshly isolated from peripheral blood were added at a concentration of 5 x 10^4 cells/well and incubated for 1 hr at 37°C. Cells stained for neutrophil markers (neutrophils were defined as high granularity SSC-A^{high}, $CD66b^+$, $CD14^-$, $CD3^-$) were analyzed by flow cytometry. A phagocytic score was determined using the percentage of $FITC^+$ cells and the mean fluorescent intensity (MFI) of the $FITC^+$ cells.

Antibody-Dependent Dendritic Cell Phagocytosis

Monocyte-derived dendritic cells (moDC) were generated from CD14+ monocytes isolated from peripheral blood and differentiated into moDC with IL-4 and GM-CSF (Miltenyi Biotec) for 6 days. Differentiation was confirmed by flow cytometry staining of CD14, CD209/DC-SIGN and CD83. Marburgvirus Ravn GP was biotinylated and conjugated to streptavidin-coated Alexa488 beads. Abs (5 μg/ml) were incubated with beads for 2 hr at 37°C prior to addition of moDCs at 1 x 10^5 cells/well and incubated with moDCs for an additional 18 hr at 37°C. moDCs were stained for surface expression of HLA-DR, CD80, and CD86 (BD Biosciences), fixed, and analyzed by flow cytometry. Expression of activation markers was determined for $FITC^+$ moDC by MFI.

Generation of Antibody Escape Mutants

To generate MR191 escape mutants, aliquots containing 100 pfu of chimeric VSV in which G was replaced with GP of MARV strain Uganda 2007 (Flyak et al., 2015) were pre-incubated with serial 2-fold dilutions starting from 200 μg/ml of MR191 mAb for 1 hr at 37°C, and then inoculated in Vero-E6 cell monolayer cultures in 96-well plates, as multiple independent replicates. After 48 hr, virus samples were harvested and titrated. For each replicate, a virus-positive preparation from the highest antibody concentration was selected for the next passage. After three passages, 200 pfu virus aliquots were pre-incubated with the highest corresponding MR191 concentrations used for the third passage, and inoculated into 24-well plate Vero-E6 cell monolayers. After 24-48 hr, based on observed cytopathic effect, virus samples were harvested and titrated, and the infected cell monolayers were lysed in 1 mL of TRIzol (Life Technologies) and subjected to total RNA isolation and sequencing of the gene encoding MARV GP.

QUANTIFICATION AND STATISTICAL ANALYSIS

Graphpad Prism software was used to determine average values, standard errors, and standard deviations. For each figure, the number of experimental replicates and other information relevant for assessing the accuracy and precision of the analysis are included in the accompanying legend.

DATA AND SOFTWARE AVAILABILITY

The structure factors and experimental model have been deposited in the RCSB Protein Data Bank under ID code PDB: 6BP2.